J Sol-Gel Sci Techn (2007) 43:47–51
DOI 10.1007/s10971-007-1534-x

Iron oxide nanoparticles within the pore system of mesoporous SBA-15 in different acidity: the synthesis and characterization

Chueh-Yang Liu · Chia-Fu Chen · Jih-Peng Leu · Yi-Chun Lin

Received: 9 July 2006 / Accepted: 2 January 2007 / Published online: 6 April 2007

Abstract Direct hydrothermal method is employed for incorporating iron into the pore structure of SBA-15. The resultant materials were analyzed by X-ray diffraction (XRD) patterns, N_2 sorption isotherm and X-ray photoelectron spectroscopy (XPS). The characterizations of XRD patterns and XPS revealed that iron nanoparticles were present as highly dispersed nanoclusters in the well-ordered mesoporous channels of SBA-15. The characterizations of t-plot reveal only microporous channels of SBA-15 are confirmed to be filled with iron nanoparticles, leaving the mesopores unaffected. The supported material still maintained its ordered mesoporous structure similar to SBA-15 and possessed high surface area, large pore volume and uniform pore size.

Keywords SBA-15 · Catalyst support · Fe_2O_3 nanoparticles · Mesoporous silica

1 Introduction

In the last decades, the synthesis and characterization of nano-sized materials have been of great interest because of their specific electronic, magnetic, optical, biological and mechanical properties compared to the bulk materials [1–4]. Template-assisted synthesis has a number of interesting and useful features for the preparation of nanostructures, since the size and shape of the desired materials can be easily directed using a well-defined template matrix [5, 6]. Among the porous materials, the mesoporous silica materials included uniform pore size distribution (2–30 nm) and high surface areas have been widely applied as host for loading catalyst [7], polymer [8], metals [9] and semiconductors [10]. Various nanoparticles have been incorporated into the frames of SBA-15 such as Al [11], Ti [12] and Zr [13–15]. In particular, their large pore size makes the nanoparticles-incorporated SBA-15 attractive as catalysts for reactions. In comparison to M41s, the SBA-15 materials which exhibit the high pore size and thick pore wall synthesized under the higher acidic conditions. Unfortunately, the synthesis conditions of SBA-15 were usually acidic, therefore, it was difficult to embed the nanoparticles. The amount of nanoparticles incorporated into the frames of SBA-15 is very low. Moreover, Newalkar and co-workers indicated the ordering of mesostructure still decreased markedly as the Zr/Si atomic ratio in the synthesis gel was greater than 5% and the mesostructure was nearly disorganized when the ratio approached 10% [15]. Li and co-workers reveal that mesostructure is still maintained when iron oxide nanoparticles are supported into SBA-15 at mild acidic conditions [16]. Fröda and co-workers reported Fe-supported SBA-15 with different precursors in dry ethanol via post-synthesis procedure and also checked the direct hydrothermal methods [17]. They found that different strategies of synthesis lead to significant changes in the bonding and environment of iron species within the silica materials. Nevertheless, some reporters showed nanoparticles supported on the SBA-15 prepared by impregnation or grafting methods are not suitable

C.-Y. Liu (✉) · J.-P. Leu
Department of Materials and Engineering,
National Chiao-Tung University,
1001 Ta Hsueh Road, Hsinchu 300, Taiwan, ROC
e-mail: jason.liu1107@msa.hinet.net

C.-F. Chen
Institute of Material and System Engineering,
MingDao University,
ChangHua 523, Taiwan, ROC

Y.-C. Lin
Department of Chemistry, National Tsing Hua University,
101, Sec 2, Kuang Fu Rd., Hsinchu 300, Taiwan, ROC

to prepare catalysts with highly isolated catalytic active sites. The studies did not present the direct hydrothermal synthesis of the Fe/SBA-15 materials. The main purpose of this work is to investigate the characterization and synthesis of Fe-nanoparticle-incorporated SBA-15 materials. The applications of multiple characterization technologies, i.e. powder X-ray diffraction (XRD), N_2 absorption spectroscopy and X-ray photoelectron spectroscopy (XPS), proved that nanostructured Fe has been formed within the pore system of SBA-15.

2 Experimental methods

2.1 Sample synthesis

The SBA-15 materials were synthesized by the traditional hydrothermal method using the triblock copolymer P123 (EO20-PO70-EO20, Aldrich) as the surfactant. In a typical synthesis, 4 g P123 was dissolved in 30 g of deionized water at 30–40 °C and stirred until transparent solution was obtained. Then, 90 g of different concentration of hydrochloric acid was added and stirred for 2 h. After 2 h, the tetraethyl orthosilicate (TEOS) and the amount of approximate $Fe(NO_3)_3 \cdot 6H_2O$ was added into the slurry. Then, the resultant solution was stirred for 20 h. The resultant solutions were quickly poured into a large polypropylene bottle. The mixture thus obtained was heated for the formation of the surfactant–silica mesophases under static conditions at 373 K. The solid products were filtered, washed with deionized water and dried at oven overnight. In order to remove the organic surfactant, the samples were calcined at 560 °C for 6 h at a heating rate of 1 K/min.

2.2 Materials characterization

XRD patterns were obtained by a Bede/D1 diffractometer using the Cu Kα radiation (1.543 Å) with a voltage of 40 kV and a current of 40 mA. The nitrogen adsorption–desorption isotherms were measured at 77 K using NOVA 1000e system in static measurement mode. The samples were degassed at 250 °C for 5 h under vacuum before measurement. The specific surface areas were calculated by Brunauer–Emmett–Teller (BET) method based on the adsorption branches. The pore diameter and pore size distribution were measured from desorption braches by the Barrett–Joyner–Halenda (BJH) method. The nanoparticles embedded analysis by XPS, using Al Kα X-ray source.

3 Results and discussion

Figure 1 show that the XRD patterns of Fe incorporated SBA-15 with Fe/Si ratios between 0.01 and 0.1. It can be seen that the XRD patterns reveal three well-ordered peaks at 0.9°, 1.6° and 1.8°, indicating well-resolved (1 0 0), (1 1 0) and (2 0 0) peaks, as shown in Fig. 1. The intensities of XRD patterns would also decrease and *d* spacing also shifts to small angle with the increase in iron loading. It seems that the absence of the prominent peaks revealed the mesostructure would collapse with high Fe loading. These effects have already been discussed in previous studies dealing with metal oxide phase within mesoporous silica [17, 18]. XRD patterns show that iron oxide nanoparticles embedded the SBA-15 templates under various acidity conditions. Well-ordered structures were observed at strongly acidic conditions. It can be seen in Fig. 2 that intensities decreased slightly with the decreasing acidic concentrations. The strong reduction of the intensities of the XRD peaks is due to

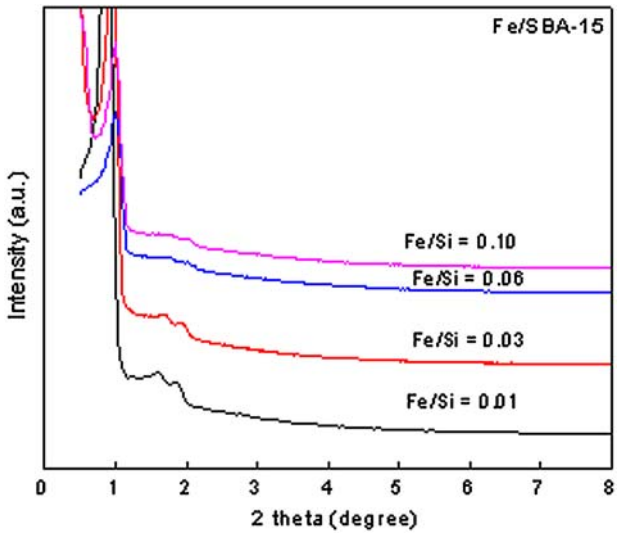

Fig. 1 Powder XRD patterns of Fe-loaded SBA-15 with various Fe/Si ratios

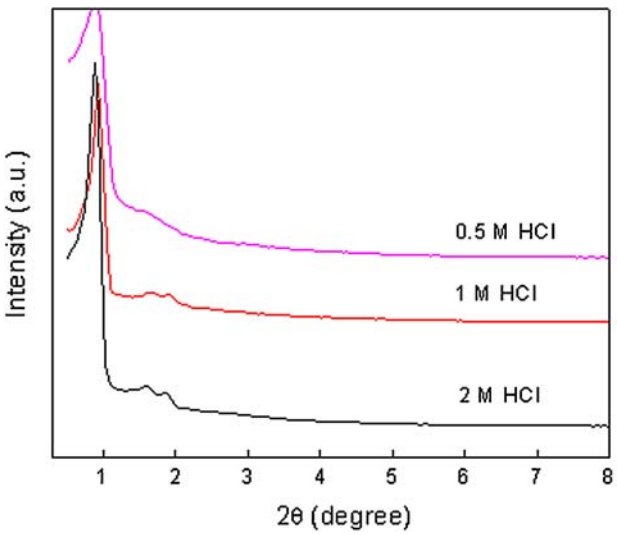

Fig. 2 Powder XRD patterns of Fe-loaded SBA-15 under various acidity conditions

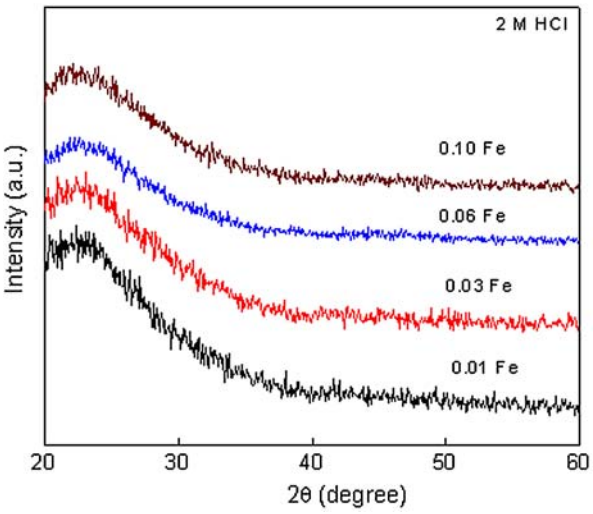

Fig. 3 High-angle XRD patterns of Fe-loaded SBA-15 with various Fe/Si ratios

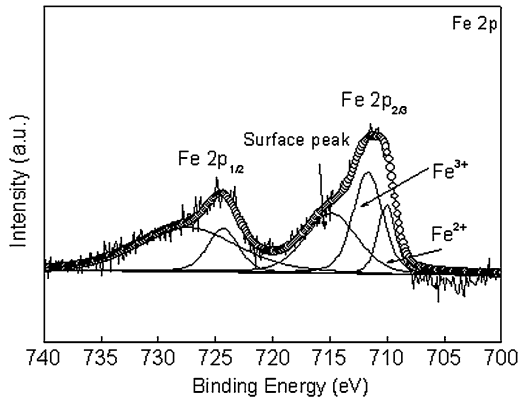

Fig. 4 XPS of Fe/SBA-15

increasing destructive interferences by filling the pores with rising amount of the iron oxide nanoparticles. In general, the introduction of scattering material into the pores lead to an increased phase cancellation between scattering from the wall and the pore regions and therefore to reduced scattering intensities for the Bragg reflections [19]. Figure 3 indicated the diffraction pattern of different iron loaded. The weak and broad reflection at $2\Theta \sim 23^\circ$ corresponds to almost amorphous SBA-15. The absence of these prominent reflections in case of the nanostructured Fe_2O_3 nanoparticles indicated that no crystalline bulk materials have been formed outside the pore system. The results also showed that Fe_2O_3 nanoparticles were dispersed uniformly in the frame of SBA-15 [20]. It reveals that protons and Fe ions are probably in a competitive position in self-assembly of the organic template and inorganic precursors. The XPS result of Fe nanoparticle is shown in Fig. 4. In the case of Fe/SBA-15, the binding energies are located at 710.0, 711.6, 714.9, 724.3 and 728.1 eV. The binding energies shifted slightly, which implies that the Fe phase in SBA-15 might be different from iron species. As a whole, the peak position is consistent with other researches [20, 21]. Wandelt et al. announced that the XPS characteristic of Fe 2p2/3 spectra is located at 707 ± 0.2 eV, 710 ± 0.2 eV and 711 ± 0.2 eV, respectively [22]. One peak located at 710.0 eV was assigned to Fe^{2+}. The peak at 711.3 eV was assigned to Fe^{3+}. These peaks are consistent with other researches [23]. Because the binding energy of Fe metal appears generally around 706.4 eV and those of the oxides are between 710 and 723 eV [24]. Accordingly, the binding energies of 714.9 eV in Fig. 4 indicate that surface energy can be assigned to Fe phase of Fe-incorporated SBA-15. Several reporters showed the peak located at 715 eV identified the surface peak [25]. Droubay and Chambers claimed that the surface peak is mostly caused by the Fe^{3+} cations at the surface of α-Fe_2O_3, which affects the binding energy of numerous samples [26]. In the bulk of iron oxides, it could be eliminated as the cause of the high binding energy surface peaks [27]. The Fe components anchored inside SBA-15 by the reaction with silanol group were oxidized through the calcinations step. However, it is believed that the iron oxide which is formed by Fe-impregnated SBA-15 might be at a different oxidation state than activated iron. Figure 5(a) shows the N_2 adsorption–desorption isotherm and pore size distribution curves determined by BET. The method gives information on the specific surface area and the pore diameter. These materials show type IV isotherm typical for the mesoporous materials [28]. A well-defined step occurs at about $p/p_0 = 0.4$; this is associated with the filling of the mesopores due to capillary condensations. All materials exhibit a sharp step at $p/p_0 = 0.6$–0.8, which demonstrates a uniform mesophase distribution. It shows that the addition of crystalline entities to mesostructured materials does not interfere with the formation of the mesoporous silica, but it disturbs the hexagonal ordering to some extent. In order to understand the textural properties of the mesoporous composites, the nitrogen isothermal sorption technology was employed to investigate the iron species effect on the pore structure as well as to determine the location of Fe in SBA-15. Figure 5(a) shows the adsorption isotherm of SBA-15 and Fe/SBA-15, with the total surface areas found to be 1091 and 912 $m^2\ g^{-1}$, respectively. In Fig. 5(a), the surface area was found to decrease somewhat from 1091 to 912 for Fe/SBA-15. Even though the SiO_2–Fe composition was observed to decrease in surface areas, this was still relatively high. Pore size distribution determined by BJH equations is shown in Fig. 5(b). It indicates that the mesoporous sizes are changing slightly from 7.00 to 6.68 nm in diameter for both SBA-15 and Fe/SBA-15. These results also show that the Fe particles do not occupy the mosoporous. From the adsorption–desorption curves, t-plots are estimated depending on the known adsorption behavior of the materials and that of non-porous standard silica (in Fig. 6) [29]. Distinct change for SBA-15 is observed, illustrating the existence of

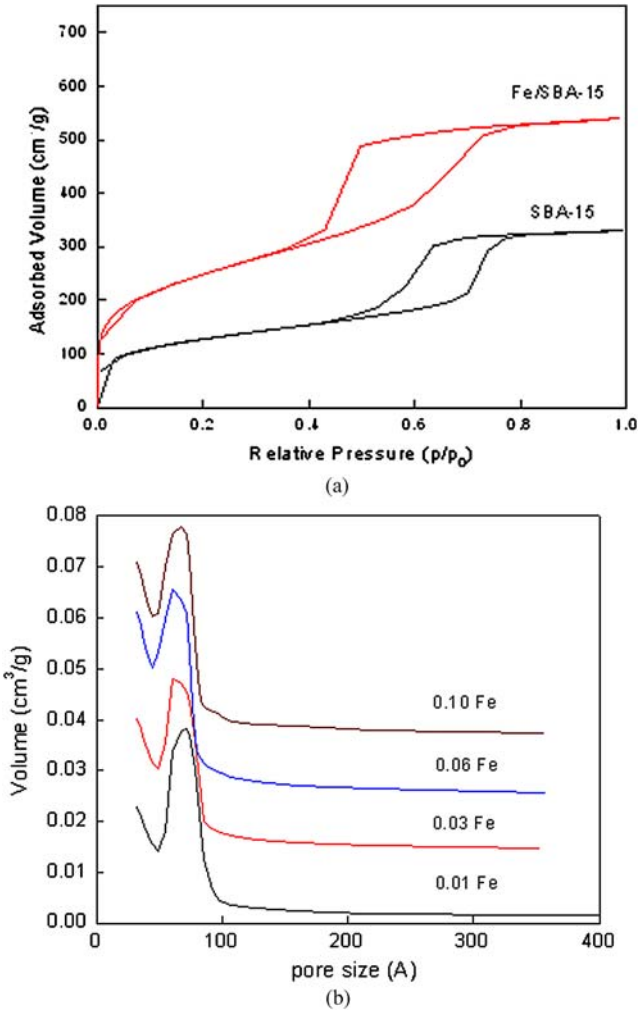

Fig. 5 Nitrogen sorption isotherms (a) and pore size distribution (b) of SBA-15 and Fe/SBA-15

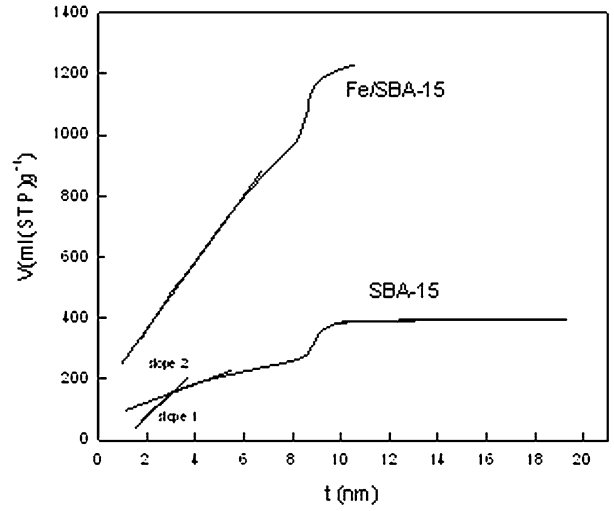

Fig. 6 t-Plot analysis of SBA-15, SBA-15-ultra and Fe/SBA-15 from nitrogen adsorption isotherms

Table 1 Surface areas and pore size distribution of SBA-15 and Fe/SBA-15 under various acidity conditions

Samples	Total surface areas (m^2/g)	Mesoporous surface area (m^2/g)	Microporous surface area (m^2/g)
SBA-15	1091	980	111
Fe/SBA-15	611	611	0

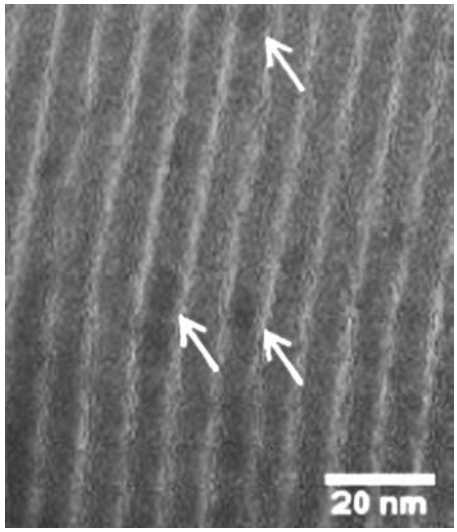

Fig. 7 Typical TEM images of the nanoparticles embedded onto the ordered mesoporous silica

microporous. On the contrary, for Fe/SBA-15, no distinct change is detected. This verifies that the micropores have disappeared after treatment of iron nitride. The microporous channels of SBA-15 are filled with Fe. Table 1 shows a detailed surface and pore size between SBA-15 and Fe/SBA-15. As shown in Table 1, there is a slight difference in total surface area between SBA-15 and Fe/SBA-15. The microporous area can be observed whereas the mesoporous surface area is almost unchanged. It is reasonable to suggest that only the microporous are filled with Fe for Fe/SBA-15 with the surface area of the mesoporous being almost the same as the original host SBA-15. On the other hand, the decrease in surface areas is likely to be principally due to plugging support pores by Fe loaded [30]. In conclusion, the t-plot reveals that Fe nanoparticles are incorporated into the microporous of SBA-15. Figure 7 shows the nanoparticles embedded onto the pore of SBA-15. It should be noted that the small amounts of iron compounds were observed in the pore of SBA-15. The diameter of these particles was equal to that of pore of SBA-15. Taking into account the XRD results, the incorporated iron species may have poor crystallinity.

4 Conclusion

In summary, highly ordered mesoporous Fe incorporating SBA-15 with different Fe contents were successfully

synthesized. Direct hydrothermal method is employed on the inner surface of self-ordered mesoporous SBA-15. The Fe loading did not affect the surface areas and pore size distribution but affected the mesostructure. Mesoporous silica SBA-15, which has high surface area and highly ordered structure, has attracted much attention as a metal nanoparticle support. Through the analysis of the resultant materials, we can find that only the micropores of SBA-15 are filled with iron metal. Therefore, a high surface area is retained after the incorporation of iron into the channels of SBA-15. The preparation method appears to be viable for template synthesis of various metal-modified mesoporous silicas with high surface areas.

Acknowledgment The authors would like to acknowledge the financial support of the National Science Council of Taiwan for this work. Acknowledgements are also extended to Center for Nano Science and Technology, NCTU for XRD experiment.

Reference

1. Alivisatos AP (1996) Science 271:933
2. Leslie-Pelecky DL, Rieke RD (1996) Chem Mater 8:1770
3. Schmid G (1992) Chem Rev 92:1709
4. Murray CB, Norris DJ, Bawendi MG (1993) J Am Chem Soc 115:8706
5. Sun L, Searson PC, Chien CL (1999) Appl Phys Chem 74: 2803
6. Lee KB, Lee SM, Cheon JW (2001) Adv Mater 13:517
7. Kim SW, Son SU, Lee SI, Hyeon T, Chung YK (2000) J Am Chem Soc 122:1550
8. Wu C, Bein T (1994) Science 264:1757
9. Plyuto Y, Berquier J, Jacquiod C, Ricolleau C (1999) Chem Commun 1653
10. Stucky GD, MacDougall JE (1990) Science 247:669
11. Kuchi V, Oliver AM, Paddon-Row MN, Howe RF (1999) Chem Commun 1149
12. Gontier S, Tuel A (1999) Appl Catal A 143:125
13. Wang MS, Huang HC, Ying JY (2002) Chem Mater 14:1961
14. Chen SY, Jang LY, Cheng SF (2004) Chem Mater 16:4174
15. Newalkar BL, Olanrewaju J, Komarneni SJ (2001) J Phys Chem B 105:8456
16. Li Y, Feng Z, Lian Y, Sun K, Zhang L, Jia G, Yang Q, Li C (2005) Micropor Mesopor Mater 84:41
17. Fröba M, Köhn R, Bouffard G (1999) Chem Mater 11:2858
18. Köhn R, Fröba M (2001) Catal Today 68:227
19. Lim MH, Blanford CF, Stein A (1998) Chem Mater 10:467
20. Martinez F, Han Y, Stucky G, Stotelo J, Ovejero G, Melero J (2002) Stud Surf Sci Catal 142:1109
21. Ruby C, Fusy J, Génin JMR (1999) Thin Solid Film 352:22
22. Wang CT, Ro SH (2006) J Non-Cryst Solid 352:35
23. Wandelt K (1982) Surf Sci Rep 2:1
24. Kim KJ, Moon DW, Lee SK, Jung KH (2000) Thin Solid Films 360:118
25. Weckhuysen BM, Wang D, Rosynek MP, Lunsford JH (1998) J Catal 175:347
26. Grosvenor AP, Kobe BA, Biesigner MC, Mclntyre NS (2004) Surf Interface Anal 36:1564
27. Droubay T, Chambers SA (2001) Phys Rev B 64:205414
28. Fujii T, de Groot FMF, Sawatzky GA, Voogt FC, Hibma T, Okada K (1999) Phys Rev B 59:3195
29. De Boer JH, Linser BG, Osinga TJ (1964) J Catal 4:643
30. Khodakov AY, Bechara R, Griboval-Constant A (2003) Appl Catal A 254:273